Synthesis and characterization of porphyrin functionalized nanodiamonds

Synthesis and characterization of porphyrin functionalized nanodiamonds

Federico Picollo[1,2,3*], Lorenzo Mino[5,2], Alfio Battiato[1], Sviatoslav Ditalia Tchernij[1,2,3], Jacopo Forneris[3], Katia Martina[4], Mirko Sacco[4], Silvia Tagliapietra[4], Ettore Vittone[1,2,3], Paolo Olivero[1,2,3], Alessandro Barge[3]

[1] Physics Department, University of Torino, via P. Giuria 1, 10125 Torino, Italy
[2] *"Nanostructured* Interfaces and *Surfaces"* (NIS) Inter-departmental Centre, University of Torino, via G. Quarello 15/a, 10135 Torino, Italy
[3] National Institute of Nuclear Physics, sect. Torino, via P. Giuria 1, 10125 Torino, Italy
[4] Department of Drug Science and Technology, University of Torino, Corso Raffaello 30, 10125 Torino, Italy
[5] Department of Chemistry, University of Torino, via Giuria 7, Torino, Italy

* Corresponding author. Email: federico.picollo@unito.it

Abstract
We report on a novel synthetic pathway for the chemical functionalization of nanodiamonds with porphyrin. To this scope, the NDs, after a thermal treatment essential to organize the crystal surface, were derivatized with reactive moieties useful to conjugate the ND with porphyrin. Untreated and modified nanoparticles were systematically characterized by X-ray photoelectron, Raman, photoluminescence and infrared spectroscopies with the purpose of evaluating the effects due to the crystals manipulation and confirming the efficacy of the proposed approach. An investigation of the effects induced to the samples by laser irradiation (probe for Raman and PL spectroscopies) was performed, highlighting the significant increase of temperature that is associated to the redshift of Raman diamond peak.

1. Introduction

In the last decades, innovative biological probes based on the unique optical and chemical properties of nanoscale materials were produced. Particularly, the employment of nanoparticles has been investigated in different environments, offering promising perspectives in biomedical research, diagnostics and therapy [1–5]. One of the most interesting materials in this context is diamond, which has received an increasing attention thanks to its very low toxicity and bio-compatibility. Furthermore, it has extremely high chemical inertness and structural stability in biological environments [6,7]. Complementarily to the above-mentioned general chemical inertness, the surface of diamond nanoparticles can be chemically decorated with a variety of functional molecules employing several different chemical processes (i.e. Diels-Alder reaction [8,9]). This opportunity is offered by the different surface termination groups that can be attached after the particle synthesis or due to specific treatments [10,11].

Nanodiamonds (NDs) derived from the fragmentation of samples produced with high-pressure high-temperature (HTHP) synthesis are characterized by a low fraction of sp^2 carbon on their surface, with respect to other synthetic methods such as detonation [12].

These nanoparticles could be used in the preparation of new sensitizer for photodynamic (PDT) or sonodynamic therapy (SDT) applications, which represent innovative approaches to treat cancer [13,14]. Both techniques are based on a similar molecular mechanism [15], which involves either

the sensitizer excitation (by light in PDT, or by ultrasound – via acoustic cavitation – in SDT) followed by reactive oxygen species (ROS) production, or by interaction with oxygen during the decay time. The produced sono/photodynamic ROS are cytotoxic and they are responsible for cells death.
Porphyrin molecules possess such physical-chemical features to be considered the first generation of sensitizers [16,17]. They are non-toxic to cell cultures [18] if they are not exposed to external stimuli as ultrasounds or light irradiation. For those reasons, they are widely used as model compounds in photo- and sono-dynamic studies.

In this study, we conjugate a porphyrin molecule to nanodiamond surface in order to develop a new hybrid nanomaterial which can represent an interesting model for PDT and SDT applications.

2. Materials and Methods

2.1 Sample fabrication

The sample under exam consists of a commercial dispersion of synthetic nanodiamond (Micron+ MDA 0-0.25, ElementSixTM) realized by means of grinding of High Pressure High Temperature (HPHT) single-crystals. The NDs are classified as type Ib, having a nominal concentration of single substitutional nitrogen comprised between 10 ppm and 100 ppm. The diamond nanoparticles size nominally ranges between a few nm and ~300 nm.
The surface of the nanocrystals presents impurities such as adsorbed contaminants or superficial amorphous layers, which are by-products of the fragmentation process. In order to re-organize the surface structure and desorb the impurities, a thermal treatment was performed.
The definition of the annealing parameters is crucial since it determines radical structural modifications: inert gas or vacuum environment avoid carbon oxidation that induces the surface termination with carbonyl and carboxyl groups, or even sample etching if temperature overcomes 500 °C in presence of an oxygen-containing atmosphere. In an oxygen-free environment, it is anyway necessary to set a temperature below 900 °C to avoid graphitization inducing the conversion of the NDs to carbon onions [19]. Therefore, the annealing process was carried out in a low-vacuum environment (pressure ~ 3 Pa) at a temperature of 800 °C for 4 hours.

The annealed NDs were then chemically functionalized adopting the pathway depicted in figure 1.

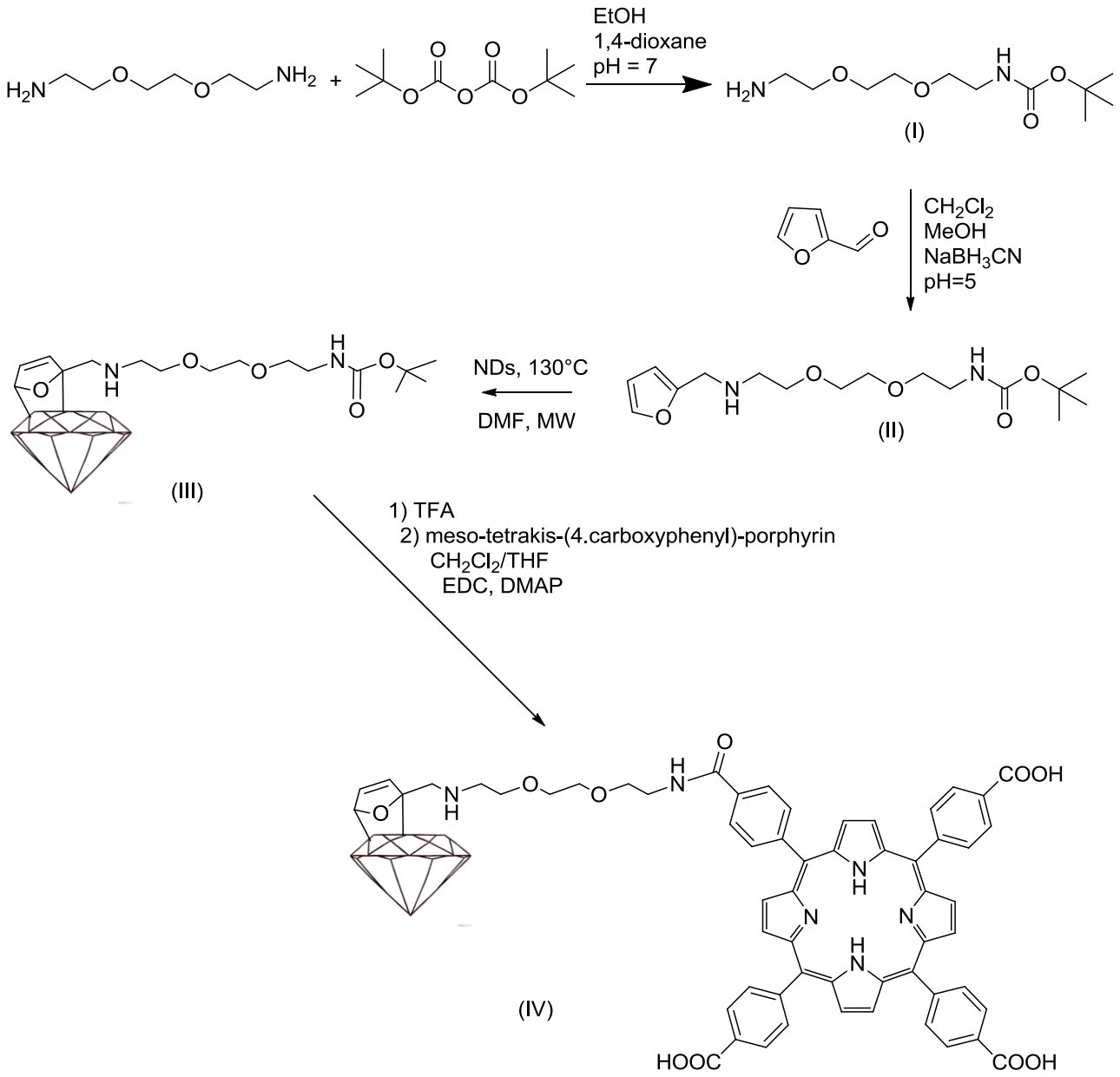

Figure 1 - Synthetic pathway to obtain hybrid nanodiamonds

Tert-butyl N-(10-(2-furanyl)-3,6-dioxa-9-azadecyl)carbamate (20 mg, 0.061 mmol) was attached to the ND surface by means of microwave enhanced synthesis.

The compound was dissolved in N,N-dimethylformamide (DMF - 10 ml), with the addition of the annealed NDs (20 mg). The mixture was heated to 130 °C for 2 hours employing a multimodal microwave reactor (Synthwave – Milestone). The solid was washed with DMF (3×10 ml) and CH_2Cl_2 (DCM - 5×10 ml) and then was dried in an oven at 100 °C for 18 hours.

The surface of the as-modified NDs is decorated with amino functional groups that can bond molecules of interest due to their higher reactivity.

After the removal of the Boc protecting group [20] (cleaved by trifluoroacetic acid, 0.35 ml for 5h at room temperature), the modified NDs were washed with DCM (5×10 ml), NaOH 1M (10 ml), and then dried in oven at 100 °C overnight. This intermediate sample was characterized only by TGA.

A solution of 5,10,15,20-tetrakis(4-carboxyphenyl)porphyrin (11 mg, 1.4 μmol), DCM (10 ml), tetrahydrofuran (THF - 2 ml), 1-Ethyl-3-(3-dimethylaminopropyl)carbodiimide (EDC - 6.1 mg, 0.084 mmol) and 4-(N,N-dimethylamino)-pyridine (DMAP - 13.6 mg, 0.112 mmol) was added to the NDs and stirred at room temperature in nitrogen atmosphere for 16 hours.

Porphyrin-functionalized NDs were separated from supernatant by centrifugation, washed with DCM (6×10 ml) and dried in oven at 100 °C overnight. The product was characterized by TGA, FTIR, XPS and Raman spectroscopy.

In the following, the description of the synthetic preparation of the reaction intermedia are reported.

Synthesis of tert-butyl N-(8-amino-3,6-dioxaoctyl)carbamate (compound I):
12 mL of 1,8-diamino-3,6-dioxaoctane were dissolved in 240 mL of a mixture of H_2O/ethanol 1:1 and the solution was cooled down to 0 °C. Maintaining the mixture temperature between 0 °C and 5 °C, a solution of tertbutyldicarbonate (12 g) in dioxane (102 ml) was slowly added, and subsequently, the reaction mixture was allowed to stir at 0 °C for 4 hours. The pH value was then adjusted to 7 by adding HCl 0.1 M and the mixture was stirred at room temperature for 24 hours. HCl 0.1 M was then added to the solution until pH value was decreased down to 4 and the mixture was extracted with DCM (3×50 ml). A second extraction with DCM (3×50 ml) was carried out after increasing pH to 9 by addition of NaOH 0.5 M solution. The organic layer resulting from the second extraction was dried over sodium sulphate and the solvent was removed under reduced pressure, obtaining the desired product as pale yellow oil in 94% yield.

Mass spectrometry (MS) and Nuclear Magnetic Resonance (NMR) were performed to confirm the synthetization of the desired compound.
MS-ESI+: calculated for $C_{11}H_{24}N_2O_4$ 248.17, found $[M+H^+]$ = 249.2, $[M+Na^+]$ = 271.2;
^{1}H NMR (600 MHz, $CDCl_3$): δ 5.17 (bs, 1H, 8), 3.60 (s, 4H, 4,5), 3.53 (t, J=6 Hz, 2H, 6), 3.51 (t, J=6 Hz, 2H, 3), 3.31 (m, 2H, 7), 2.88 (t, J=6Hz, 2H, 2), 1.64 (s, 2H, 1), 1.43 (s, 9H, 9,10,11).
^{13}C-NMR (6000 MHz, $CDCl_3$ 77) δ156.0, 79.2, 70.1, 53.4, 4.4, 41.3, 40.3, 28.4. (Spectra are reported in the supporting information).

Synthesis of tert-butyl N-(10-(2-furanyl)-3,6-dioxa-9-azadecyl)carbamate (compound II):
Compound I (202 mg, 8.149×10^{-4} mol) was dissolved in methanol (7 ml) and then the pH was adjusted to 5 by adding HCl 0.1 M. A solution of freshly distilled furfural (45 µl, 5.433×10^{-4} mol) in DCM (7 ml) was added to the mixture and stirred at room temperature for 2 hours. Then, solid $NaBH_3CN$ (51 mg, 8.149×10^{-4} mol) was added stepwise (3 portions, one each 30 min) maintaining the pH value around 5. After stirring for 12 hours, the solvent was removed under vacuum, the residue dissolved in DCM (15 ml) and washed with water (15 ml). The aqueous layer was extracted with DCM (3×15 ml), the organic phases were combined, dried over sodium sulphate and subsequently the solvent was removed. The final product was recovered as dark yellow oil in 62% yield.

Mass spectrometry (MS) and Nuclear Magnetic Resonance (NMR) were performed to confirm the synthetization of the desired compound.
MS ESI+: calculated for $C_{16}H_{28}N_2O_5$ 328.20, found $[M+H^+]$ = 329.41, $[M+Na^+]$ = 351.41;
^{1}H NMR (600 MHz, $CDCl_3$): δ 7.38 (s, 1H, 1), 6.33 (s, 1H, 2), 6.29 (s, 1H, 3) 5.18 (s, 1H, 12), 3.90 (s, 2H, 4), 3.61 (m, 4H, 8,9), 3.54 (t, J = 6Hz, 2H, 10), 3.48 (m, 2H, 7), 3.30 (m, 2H, 11), 2.87 (s, 2H, 6), 1.43 (s, 9H, 13,14,15).
^{13}C-NMR (600 MHz, CDCl3 77.00) δ 156.1, 154.2, 142.8, 110.7, 108.0, 70.3, 57.5, 48.1, 45.2, 40.5, 28.6 (Spectra are reported in the supporting information).

2.2 Sample characterization

Thermogravimetric measurements were carried out on TGA 4000 Analyzer (Perkin Elmer), under argon atmosphere, in a temperature range between 50 °C and 800 °C. Temperature increase rate was set to 10 °C min^{-1}.

X-ray Photoelectron Spectroscopy (XPS) analysis was performed with a VSW TA10 non-monochromatic Al x-ray source (K_α energy: 1.4866 keV) equipped with a VSW Class 100 Concentric Hemispherical Analyser in ultra-high vacuum conditions (~ 10^{-7} Pa) with a detection limit of the order of 1%. A thin layer of NDs was placed into a small container coated with gold in order to mitigate both charge effects and the contamination of adventitious carbon, suitably designed for powder samples (see figure 2A). In XPS measurements the sample under analysis must be electrically conductive in order to avoid charge effects, which can introduce a shift in peaks position or hide features related to the chemical nature of the observed elements. Moreover, before analysis nanoparticle was placed in a load chamber where it was heated up to 120 °C for 3 hours at a pressure of 10^{-4} Pa to fully remove any absorbed water.

Raman and Photoluminescence (PL) spectra were acquired with a Horiba Jobin Yvon HR800 Raman micro-spectrometer equipped with two alternative diffraction gratings, characterized respectively by 600 lines mm^{-1} and 1800 lines mm^{-1}. The optical excitation was provided by a continuous 532 nm laser focused with a 100× air objective. The excitation radiation was filtered out from the CCD detection system by a narrow-band notch filter (Super Notch Plus 532 nm filter, 6.0 optical density, 10 nm spectral bandwidth). The employed magnification allowed to probe the entire volume of isolated NDs or small aggregates, since the laser spot is 2 μm both in diameter and in focal depth. The spectrometer also allows controlling the laser power intensity in the 0.05 – 4.11 mW range, inserting different filters along the excitation optical path.

An Inspect F™ scanning electron microscope (SEM) was used to investigate the morphological features of the ND samples. The system is equipped with a Field Emission Gun (FEG), which allows a nominal ~3 nm lateral resolution at a 1 kV accelerating voltage. The samples under analysis were not metal coated: although leading to possible charging effects, this allowed to avoid any modification of NDs morphology. A 5 keV electron beam was employed, ensuring a good topographical contrast and satisfactory spatial resolution.

FT-IR spectra were acquired using a Bruker Equinox 55 spectrometer equipped with a Spectra Tech DRIFT accessory (model 0030-011) and a MCT detector. The samples were measured under a dry air flux in order to minimize the fluctuation of water vapour in the analysis chamber, thus avoiding the formation of artefacts. Each spectrum was collected in diffuse reflectance mode by averaging 64 interferograms at 2 cm^{-1} spectral resolution, and successively converted into pseudo-absorbance units (i.e. A = - log R, R being the reflectance).

3. Results

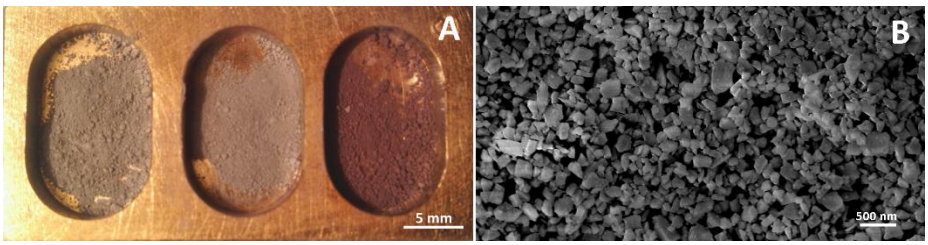

Figure 2 – A) optical image of ND layers placed in the XPS sample holder. The batches consist of (from left to right): untreated, annealed and porphyrin-functionalized NDs. B) SEM micrograph of untreated NDs.

Figure 2A shows optical images of the ND layers in the XPS sample holder. A slight difference in colour is visible between the batches of untreated NDs (left) and annealed NDs (centre): the latter one appears as clearer, suggesting the removal of surface contamination introduced during the production synthesis. The colour variation between the annealed NDs (centre) and the porphyrin-functionalized NDs (right) is more clearly visible and represents a first evidence of the surface modification.
The SEM micrograph in figure 2B shows the annealed NDs: the distribution in NDs size ranges from few nanometers up to 300 nm, consistently with those reported by the supplier. The NDs with smaller dimensions are usually aggregated with the larger ones.

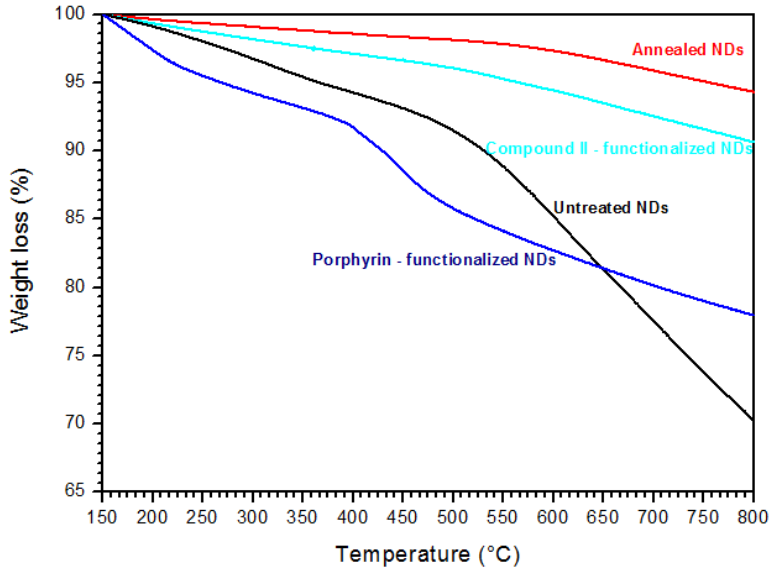

Figure 3 – Thermogravimetric analysis of untreated (black), annealed (red), compound II functionalized (cyan) and porphyrin-functionalized (blue) NDs.

Thermogravimetric analysis provides information about the thermal stability of surface groups and the degree of functionalization after derivatization. Figure 3 shows the higher stability of the annealed NDs with respect to the untreated NDs, in which the pronounced weight loss could be associated to the reduction of carboxylic, carbonyl and hydroxyl groups (see FT-IR section).
Simultaneously, annealed NDs offer a highly extended sp^2 surface that can be efficiently derivatized; in fact, a derivatization degree of 3.4% w/w is obtained for the functionalization of NDs with tert-butyl N-(10-(2-furanyl)-3,6-dioxa-9-azadecyl)carbamate and a derivatization degree of 15.7% w/w after the conjugation of porphyrin. Derivatization amount has been calculated from weight loss percentage differences at 700°C (both the percentage are evaluated with respect to untreated ND). The thermogravimetric profiles of the two surface modified ND suggest a covalent interaction between linker (compound II) and ND surface and between porphyrin and linker. However, to exclude different kind of interactions or reactions, annealed NDs were mixed with porphyrin in the same conjugation reaction condition, with and without the presence of EDC. TGA profiles of this treated NDs are fully superimposable to the annealed pristine (see supplementary information).

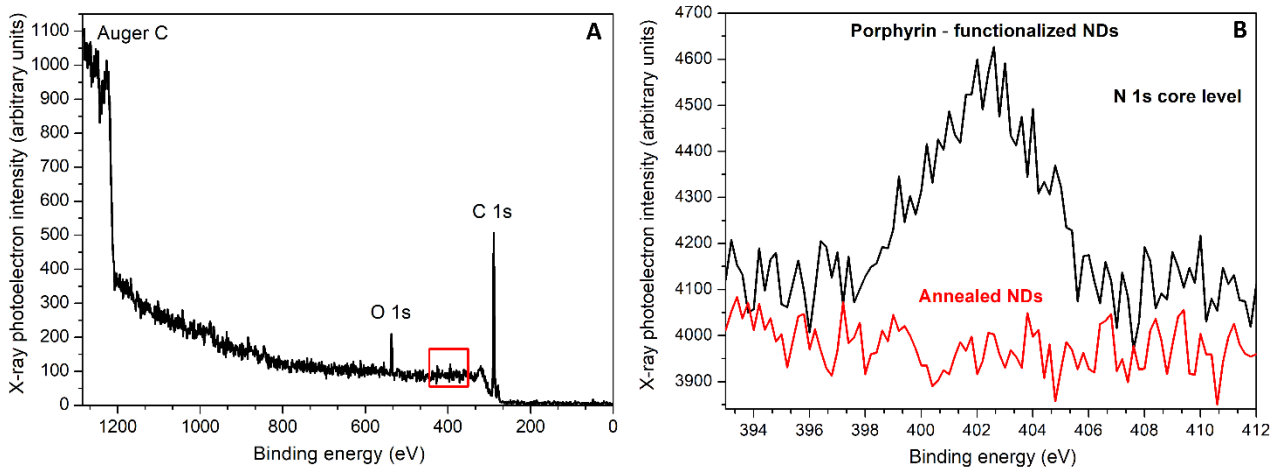

Figure 4 – A) Survey XPS spectrum of a porphyrin-functionalized ND layer. B) Zoom of the XPS spectrum reported in A (spectral region highlighted by the red square); the N1s core line is clearly visible for the porphyrin-functionalized NDs (black line), while it is absent from the annealed NDs (red line).

The chemical functionalization affects only the surface of the NDs, therefore a surface-sensitive technique such as X-Ray Photon Spectroscopy is ideal to investigate it. Survey XPS spectra were acquired at binding energies ranging between 0 eV and 1200 eV, using a fixed 44 eV pass energy at the hemispherical analyser, with step energy of 1 eV and integration time of 1 s. These acquisition parameters guarantee to identify the main chemical species present on the NDs surface. Figure 4A reports a survey XPS spectrum acquired for the porphyrin-functionalized NDs, but similar features were also observed for the other samples and therefore not reported here. Only the presence of the main peak (1s) of C and O is clearly identifiable within the detection sensitivity. High-resolution spectra of the C 1s and O 1s core lines (carried at 22 eV pass energy and 0.2 eV step energy) did not provide further information of possible chemical shifts because of the presence of charging effects. The presence of nitrogen in the porphyrin-functionalized NDs was investigated to confirm the effectiveness of the chemical surface modification since this heteroatom is both present in the linker and in the porphyrin. The relative concentration of this element with respect to oxygen and carbon is known and is close to the detection limit of the instrumentation; therefore, in order to work with feasible acquisition times, a 44 eV pass energy was set, thus slightly decreasing the energy resolution in favour of an increased number of counts. The comparison between XPS spectra from annealed-only and porphyrin-functionalized NDs in the N 1s binding energy region (415 – 385 eV) is reported in figure 4B, showing a clear evidence of the successful functionalization.

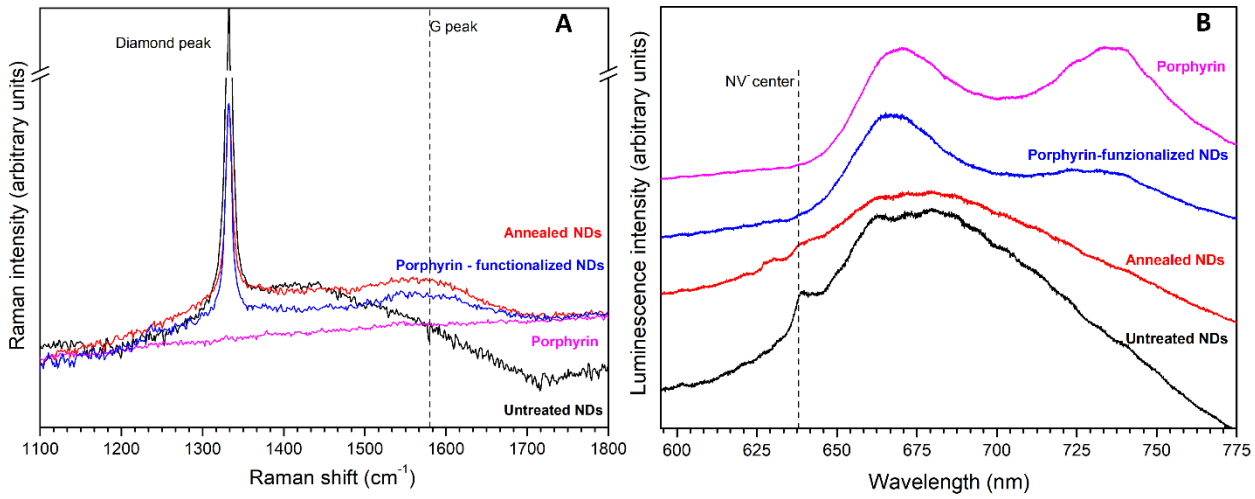

Figure 5 – Micro-Raman (A) and photoluminescence (B) spectra collected at 1.21 mW laser excitation power from untreated NDs (black line), annealed NDs (red line), porphyrin-functionalized NDs (blue line) and porphyrin (magenta line). Significant features are highlighted and labelled (note: the graph in panel A are plotted with a semi-logarithmic scale, the graph in panel B are vertically displaced for sake of readability).

Raman and PL spectroscopies were performed respectively to assess possible structural modifications induced to the NDs and to further confirm the success of the functionalization process. Figure 5A shows the Raman spectra collected from different ND samples (untreated, annealed-only and functionalized NDs) upon an excitation laser power of 1.21 mW and 600 lines mm^{-1} diffraction grating. As expected, all the samples present the first-order Raman peak of diamond (1332 cm^{-1}), while features related to graphitic or amorphous carbon can be identified for both the annealed-only and the porphyrin-functionalized NDs. These features are the widely observed D and G bands located at ~1350-1450 cm^{-1} and 1550-1650 cm^{-1}, respectively [21]. G band appear after the thermal annealing, thus suggesting the surface reorganization of the NDs by increasing the fraction of sp^2-bonded carbon. Notably, these features do not show appreciable variations after the functionalization, indicating a negligible further alteration of the material upon this process.

Most importantly, as shown in figure 5B, porphyrin-functionalized NDs presents two broad PL peaks centred at ~670 nm and ~735 nm, which are fully consistent with similar features observed in the spectrum acquired from the reference porphyrin sample. This experimental evidence, combined with the results of XPS measurements, represents a further confirmation of the successful functionalization of the NDs.

In addition, as shown in figure 5B, the PL spectra from untreated and annealed-only NDs show features ascribable to a high concentration of negatively-charged nitrogen-vacancy defects (NV^-, 638 nm zero-phonon line). As widely observed, the zero phonon line of the NV^- is associated with a broad phonon sideband in the 650-750 nm spectral range. The NV^- emission is easily measurable for the untreated NDs, while the formation of superficial graphitic phases in annealed NDs degrades its spectral quality, which exhibits a significantly weaker zero-phonon line. As expected, also porphyrin-functionalized NDs do not exhibit any NV^- luminescence (both zero-phonon line and phonon sideband), but the porphyrin emission only.

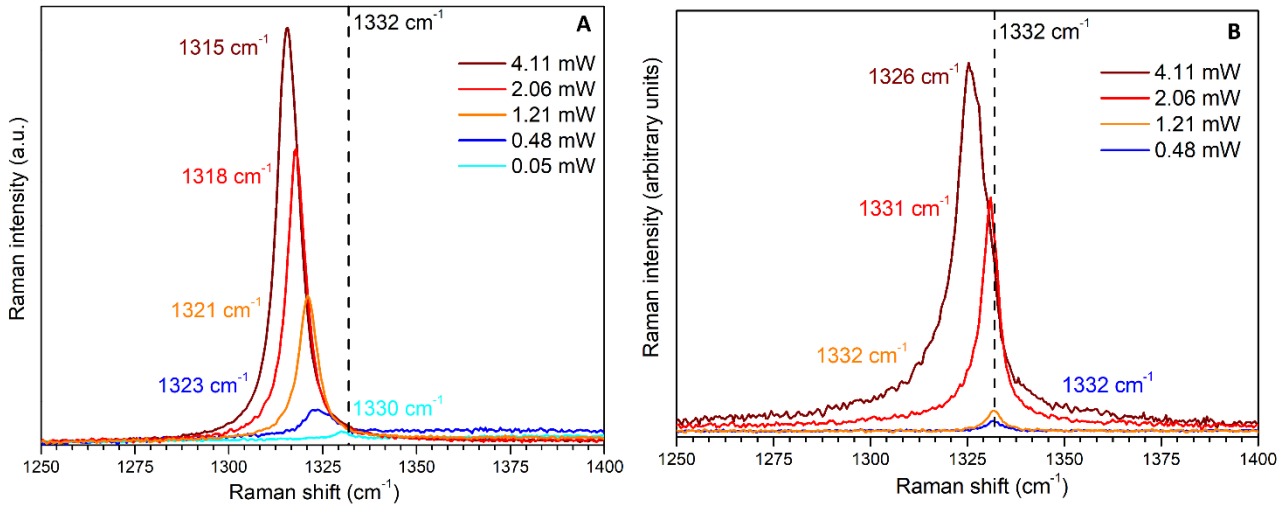

Figure 6 - First-order diamond Raman peak of porphyrin-functionalized NDs (A) and annealed NDs (B) acquired at different laser excitation powers: a redshift at increasing power is clearly visible.

Figure 6A shows spectra of the first-order Raman peak from the porphyrin-functionalized NDs collected with different excitation laser power values, at increased spectral resolution (1800 cm^{-1} grating). Remarkably, the Raman peak exhibits an increasing red-shift at increasing laser power intensities: at low excitation power (0.05 mW) a 2 cm^{-1} redshift can be appreciated, while at the maximum excitation power achievable (4.11 mW) the first-order diamond line is detected at 1315 cm^{-1}. Consistently with what reported in ref. [22,23], laser irradiation can induce heating of the nanoparticle, thus significantly affecting the position of the diamond Raman peak. As shown in figure 6B, this effect is also observed in untreated NDs, although with significantly smaller red-shifts (0-6 cm^{-1} for the same excitation power range); this is attributed to the fact that the functional groups increase the optical absorption of the NDs and consequently their temperature under illumination. The strong optical absorption of the porphyrin moiety is confirmed by the fact that the functionalized NDs show a negligible NV^- emission, despite the fact that the concentration of these defects in the NDs can be reasonably expected to be largely unaffected by the surface functionalization.

The redshift effect can be explained assuming an anharmonic decay channel of the excited optical phonon into two acoustic phonons but with opposite momenta which downshift the Raman peak frequency with respect to the value 1332.7 cm^{-1} [24]. This contribution is temperature dependent.

The temperature reached by the NDs under laser irradiation at higher power can be estimated as comprised between 400 °C and 650 °C, based on the following considerations. The former value can be inferred by considering the degradation temperature of porphyrin obtained from the thermogravimetric analysis, an effect that is observable after just few minutes at higher irradiation power. The latter value was obtained by comparing our results with the empirical relationship (I) reported in [22], which correlate the Raman red-shift with sample temperature:

(I)

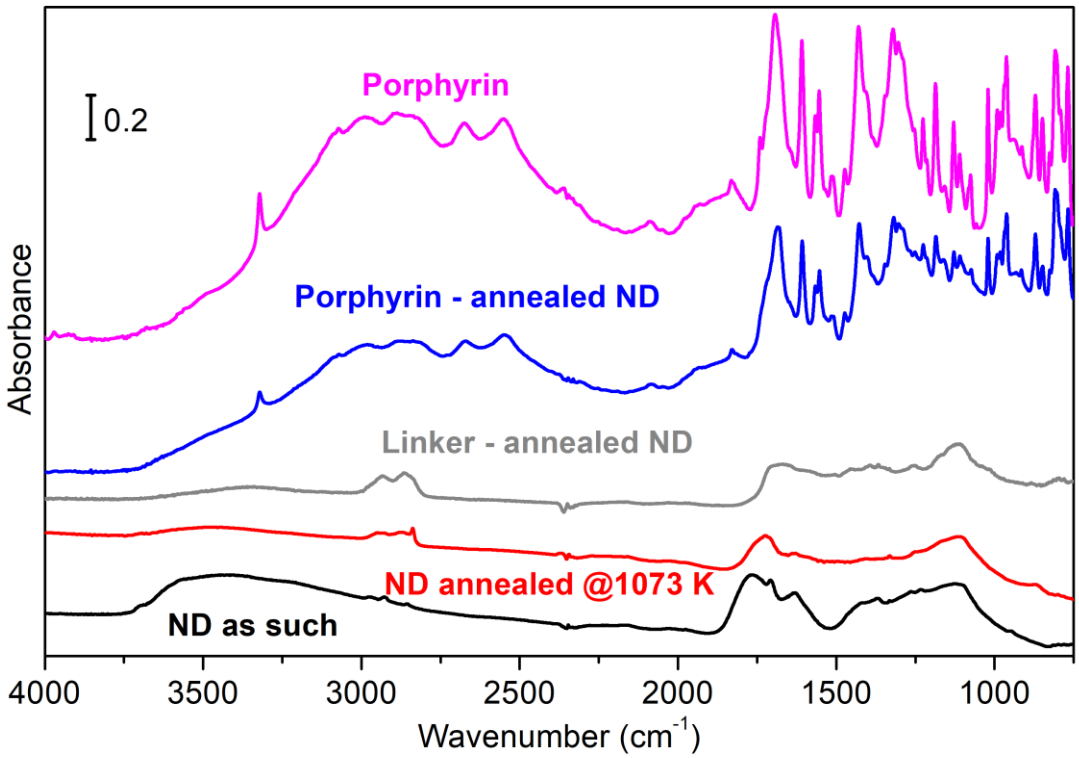

Figure 7 - FT-IR spectra of untreated (black), annealed (red) compound II-functionalized (grey) and porphyrin-functionalized (blue) NDs. The porphyrin spectrum (magenta) is also reported for reference. A magnification of untreated and annealed NDs spectra is available in the figure S7 of supporting information.

FT-IR spectroscopy provides information about the modification of the surface functional groups resulting from the annealing of the pristine NDs and also allows investigating the surface-porphyrin interaction in the functionalized NDs [25,26]. The spectrum of the untreated NDs (black curve in figure 7) is characterized by the presence of a broad absorption in the 3650-3000 cm^{-1} spectral region, associated to the ν(O-H) stretching modes of hydrogen bonded water molecules, which give also rise to the band of the $\delta(H_2O)$ bending mode at 1630 cm^{-1} [27–29]. The weak signals in the 2990-2820 cm^{-1} range can be ascribed to ν(C-H) stretching modes, while the band at 1765 cm^{-1} is due to ν(C=O) vibrations [30]. From the spectra of the annealed NDs increasing in the number of C-H moieties and a parallel decrease of the C=O groups is observable. This results in a lower affinity of the surface towards water, as indicated by the evident decrease in intensity of the ν(O-H) and $\delta(H_2O)$ signals. Concerning the effect of functionalization, the introduction of the linker minimally modify the spectra due to the absence of specific resonances. Magnified spectra for untreated, annealed and linker-functionalized nanodiamonds are reported in figure S7 of supporting information.

Meanwhile, by comparing the FT-IR spectra of pure porphyrin and of the functionalized ND (magenta and blue curves in figure 7, respectively), it can be observed that the main spectral features - e.g. the narrow band at 3321 cm^{-1} due to the ν(N-H) stretching and the vibrations

involving C=C and C=N stretchings of the porphyrin macrocycle in the region between 1650 and 1400 cm^{-1} [31] - are very similar. This observation suggests that the majority of the chemical bonds in the porphyrin are weakly perturbed by the interaction with the surface. However, a change in band shape and a frequency shift of the main peak from 1693 cm^{-1} to 1682 cm^{-1} can be observed for the carbonyl stretching signal.

Conclusions

In the present work, we reported on the chemical functionalization of nanoparticles obtained by the fragmentation of HPHT diamond crystals, by covalent bonding of porphyrin on their surface through a linker. The samples were systematically characterized with thermogravimetry, as well as with XPS, micro-Raman/PL and FT-IR spectroscopies following each processing step, demonstrating the efficacy of the proposed functionalization pathway.
In parallel, a detailed characterization of laser heating effects was also described, underlying the importance of setting the laser power during Raman spectroscopy in order to avoid functional group thermal degradation.

Acknowledgements

This research was supported under the following schemes: “DIACELL” project funded by the Italian National Institute of Nuclear Physics (INFN) - CSN5, “MiraDS” project funded by the CRT Foundation and "Departments of Excellence" project (L. 232/2016), funded by the Italian Ministry of Education, University and Research (MIUR) and “Diamond Microfabrication” experiment at the “Nanofacility Piemonte” laboratory of INRiM.

References

[1] M. Auffan, J.J. Rose, J.-Y.Y. Bottero, G. V. Lowry, J.-P.P. Jolivet, M.R. Wiesner, Towards a definition of inorganic nanoparticles from an environmental, health and safety perspective, Nat. Nanotechnol. 4 (2009) 634–641. doi:10.1038/nnano.2009.242.

[2] M.E. Davis, Z. (Georgia) Chen, D.M. Shin, Nanoparticle therapeutics: an emerging treatment modality for cancer, Nat. Rev. Drug Discov. 7 (2008) 771–782. doi:10.1038/nrd2614.

[3] I. Corazzari, A. Gilardino, S. Dalmazzo, B. Fubini, D. Lovisolo, Localization of CdSe/ZnS quantum dots in the lysosomal acidic compartment of cultured neurons and its impact on viability: Potential role of ion release, Toxicol. Vitr. 27 (2013) 752–759. doi:10.1016/j.tiv.2012.12.016.

[4] R.A. Petros, J.M. DeSimone, Strategies in the design of nanoparticles for therapeutic applications, Nat. Rev. Drug Discov. 9 (2010) 615–627. doi:10.1038/nrd2591.

[5] L. Mino, G. Agostini, E. Borfecchia, D. Gianolio, A. Piovano, E. Gallo, C. Lamberti, Low-dimensional systems investigated by x-ray absorption spectroscopy: a selection of 2D, 1D and 0D cases, J. Phys. D. Appl. Phys. 46 (2013) 423001. doi:10.1088/0022-3727/46/42/423001.

[6] R. Schirhagl, K. Chang, M. Loretz, C.L. Degen, Nitrogen-Vacancy Centers in Diamond: Nanoscale Sensors for Physics and Biology, Annu. Rev. Phys. Chem. 65 (2014) 83–105. doi:10.1146/annurev-physchem-040513-103659.

[7] L. Guarina, C. Calorio, D. Gavello, E. Moreva, P. Traina, A. Battiato, S. Ditalia Tchernij, J. Forneris, M. Gai, F. Picollo, P. Olivero, M. Genovese, E. Carbone, A. Marcantoni, V. Carabelli,

Nanodiamonds-induced effects on neuronal firing of mouse hippocampal microcircuits, Sci. Rep. 8 (2018) 2221. doi:10.1038/s41598-018-20528-5.
[8] G. Jarre, Y. Liang, P. Betz, D. Lang, A. Krueger, Playing the surface game - Diels-Alder reactions on diamond nanoparticles, Chem. Commun. 47 (2011) 544–546. doi:10.1039/c0cc02931a.
[9] F. Bosca, L. Orio, S. Tagliapietra, I. Corazzari, F. Turci, K. Martina, L. Pastero, G. Cravotto, A. Barge, Microwave-Assisted Synthesis and Physicochemical Characterization of Tetrafuranylporphyrin-Grafted Reduced-Graphene Oxide, Chem. - A Eur. J. 22 (2016) 1608–1613. doi:10.1002/chem.201503887.
[10] S. Osswald, G. Yushin, V. Mochalin, S.O. Kucheyev, Y. Gogotsi, Control of sp2/sp3 carbon ratio and surface chemistry of nanodiamond powders by selective oxidation in air, J. Am. Chem. Soc. 128 (2006) 11635–11642. doi:10.1021/ja063303n.
[11] A. Krueger, New carbon materials: Biological applications of functionalized nanodiamond materials, Chem. - A Eur. J. 14 (2008) 1382–1390. doi:10.1002/chem.200700987.
[12] S. Stehlik, M. Varga, M. Ledinsky, V. Jirasek, A. Artemenko, H. Kozak, L. Ondic, V. Skakalova, G. Argentero, T. Pennycook, J.C. Meyer, A. Fejfar, A. Kromka, B. Rezek, Size and Purity Control of HPHT Nanodiamonds down to 1 nm, J. Phys. Chem. C. 119 (2015) 27708–27720. doi:10.1021/acs.jpcc.5b05259.
[13] I. Rosenthal, J.Z. Sostaric, P. Riesz, Sonodynamic therapya review of the synergistic effects of drugs and ultrasound, Ultrason. Sonochem. 11 (2004) 349–363. doi:10.1016/j.ultsonch.2004.03.004.
[14] Y.Y. Liu, G. Wan, H. Guo, Y.Y. Liu, P. Zhou, H. Wang, D. Wang, S. Zhang, Y. Wang, N. Zhang, A multifunctional nanoparticle system combines sonodynamic therapy and chemotherapy to treat hepatocellular carcinoma, Nano Res. 10 (2017) 834–855. doi:10.1007/s12274-016-1339-8.
[15] G.-Y. Wan, Y. Liu, B.-W. Chen, Y.-Y. Liu, Y.-S. Wang, N. Zhang, G.-Y. Wan, Y. Liu, B.-W. Chen, Y.-Y. Liu, Y.-S. Wang, N. Zhang, Recent advances of sonodynamic therapy in cancer treatment, Cancer Biol. Med. 13 (2016) 325–338. doi:10.20892/j.issn.2095-3941.2016.0068.
[16] G. Varchi, F. Foglietta, R. Canaparo, M. Ballestri, F. Arena, G. Sotgiu, A. Guerrini, C. Nanni, G. Cicoria, G. Cravotto, S. Fanti, L. Serpe, Engineered porphyrin loaded core-shell nanoparticles for selective sonodynamic anticancer treatment, Nanomedicine. 10 (2015) 3483–3494. doi:10.2217/nnm.15.150.
[17] S. Endo, N. Kudo, S. Yamaguchi, K. Sumiyoshi, H. Motegi, H. Kobayashi, S. Terasaka, K. Houkin, Porphyrin Derivatives-Mediated Sonodynamic Therapy forMalignant Gliomas InVitro, Ultrasound Med. Biol. 41 (2015) 2458–2465. doi:10.1016/j.ultrasmedbio.2015.05.007.
[18] W. Xiong, P. Wang, J. Hu, Y. Jia, L. Wu, X. Chen, Q. Liu, X. Wang, A new sensitizer DVDMS combined with multiple focused ultrasound treatments: an effective antitumor strategy, Sci. Rep. 5 (2015) 17485. doi:10.1038/srep17485.
[19] A. Krueger, D. Lang, Functionality is key: Recent progress in the surface modification of nanodiamond, Adv. Funct. Mater. 22 (2012) 890–906. doi:10.1002/adfm.201102670.
[20] T. Takimoto, T. Chano, S. Shimizu, H. Okabe, M. Ito, M. Morita, T. Kimura, T. Inubushi, N. Komatsu, Preparation of fluorescent diamond nanoparticles stably dispersed under a physiological environment through multistep organic transformations, Chem. Mater. 22 (2010) 3462–3471. doi:10.1021/cm100566v.
[21] J. Filik, J. Hodkiewicz, T.F. Scientific, T.R. Society, P. Transactions, E. Sciences, I. Childres, L. Jauregui, W. Park, H. Cao, Y. Chen, J. B. Lambert, Raman spectroscopy : a the lightest touch, Spectrosc. Eur. 17 (2005) 10–16. doi:10.1088/0022-3727/46/12/122001.
[22] T.A. Nachal'naya, V.D. Andreyev, E. V. Gabrusenok, Shift of the frequency and Stokes-anti-

Stokes ratio of Raman spectra from diamond powders, Diam. Relat. Mater. 3 (1994) 1325–1328. doi:10.1016/0925-9635(94)90146-5.
[23] M. Chaigneau, G. Picardi, H.A. Girard, J.C. Arnault, R. Ossikovski, Laser heating versus phonon confinement effect in the Raman spectra of diamond nanoparticles, J. Nanoparticle Res. 14 (2012). doi:10.1007/s11051-012-0955-9.
[24] Q.Y. Liu, M. Coulombe, J. Dumm, K.M. Shaffer, A.E. Schaffner, J.L. Barker, J.J. Pancrazio, D. a. Stenger, W. Ma, Synaptic connectivity in hippocampal neuronal networks cultured on micropatterned surfaces, Dev. Brain Res. 120 (2000) 223–231. doi:10.1016/S0165-3806(00)00014-6.
[25] A. Wang, W. Yu, Z. Huang, F. Zhou, J. Song, Y. Song, L. Long, M.P. Cifuentes, M.G. Humphrey, L. Zhang, J. Shao, C. Zhang, Covalent functionalization of reduced graphene oxide with porphyrin by means of diazonium chemistry for nonlinear optical performance, Sci. Rep. 6 (2016) 23325. doi:10.1038/srep23325.
[26] L. Mino, IR spectroscopy as a tool to investigate photocatalytic reactions at oxide surfaces, Rend. Lincei. 28 (2017) 143–149. doi:10.1007/s12210-016-0592-9.
[27] S. Ji, T. Jiang, K. Xu, S. Li, FTIR study of the adsorption of water on ultradispersed diamond powder surface, Appl. Surf. Sci. 133 (1998) 231–238. doi:10.1016/S0169-4332(98)00209-8.
[28] L. Mino, G. Spoto, S. Bordiga, A. Zecchina, Particles morphology and surface properties as investigated by HRTEM, FTIR, and periodic DFT calculations: From pyrogenic TiO 2 (P25) to nanoanatase, J. Phys. Chem. C. 116 (2012) 17008–17018. doi:10.1021/jp303942h.
[29] S. Bordiga, C. Lamberti, F. Bonino, A. Travert, F. Thibault-Starzyk, Probing zeolites by vibrational spectroscopies, Chem. Soc. Rev. 44 (2015) 7262–7341. doi:10.1039/C5CS00396B.
[30] G.A. Inel, E.M. Ungureau, T.S. Varley, M. Hirani, K.B. Holt, Solvent-surface interactions between nanodiamond and ethanol studied with in situ infrared spectroscopy, Diam. Relat. Mater. 61 (2016) 7–13. doi:10.1016/j.diamond.2015.11.001.
[31] L.J. Boucher, J.J. Katz, The Infared Spectra of Metalloporphyrins (4000-160 Cm-1), J. Am. Chem. Soc. 89 (1967) 1340–1345. doi:10.1021/ja00982a011.

Supplementary Information

Synthesis and characterization of porphyrin functionalized nanodiamonds

F. Picollo[1,2,3*], L. Mino[5,2], A. Battiato[1], S. Ditalia Tchernij[1,2,3], J. Forneris[3], K. Martina[4], M. Sacco[4], S. Tagliapietra[4], E. Vittone[1,2,3], P. Olivero[1,2,3], A. Barge[3]

[1] Physics Department, University of Torino, via P. Giuria 1, 10125 Torino, Italy
[2] *"Nanostructured* Interfaces and *Surfaces"* (NIS) Inter-departmental Centre, University of Torino, via G. Quarello 15/a, 10135 Torino, Italy
[3] National Institute of Nuclear Physics, sect. Torino, via P. Giuria 1, 10125 Torino, Italy
[4] Department of Drug Science and Technology, University of Torino, Corso Raffaello 30, 10125 Torino, Italy
[5] Department of Chemistry, University of Torino, via Giuria 7, Torino, Italy

* Corresponding author. Email: federico.picollo@unito.it

Summary

Characterization of tert-butyl-(2-(2-(2-ethoxyamino)-ethoxy)-ethyl)-carbamate (compound I):

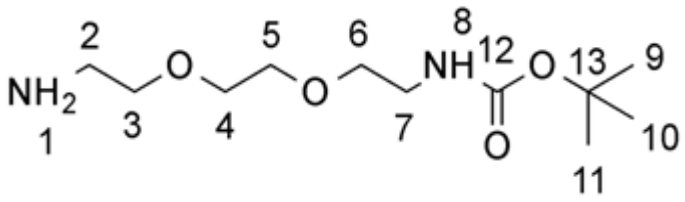

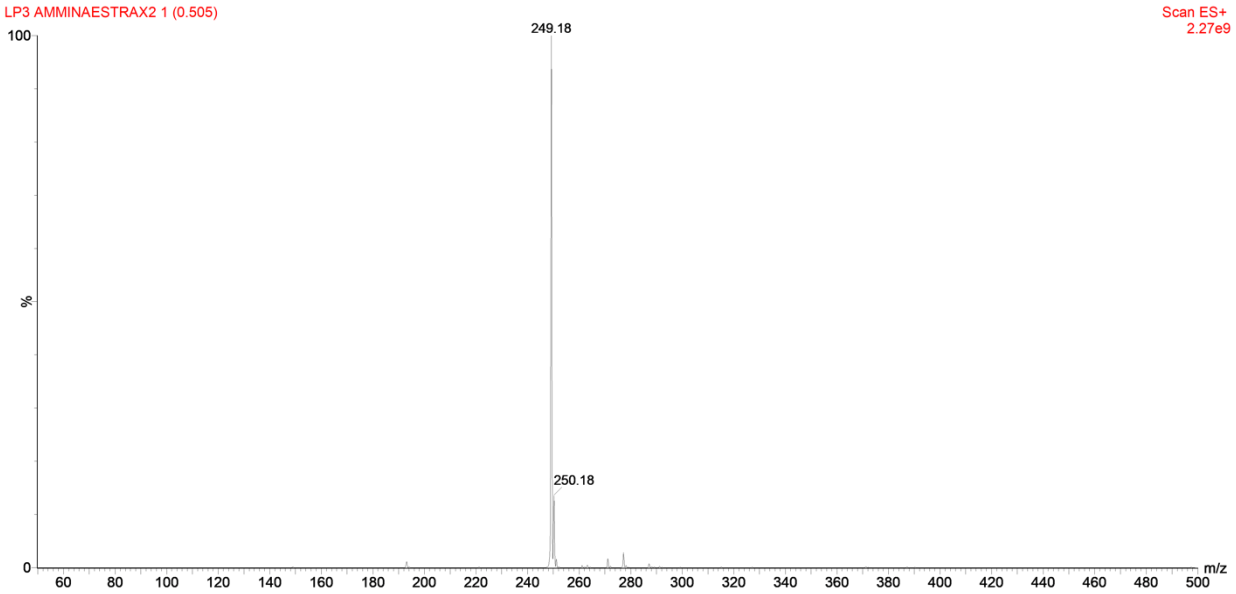

Figure S1: MS spectrum of compound I

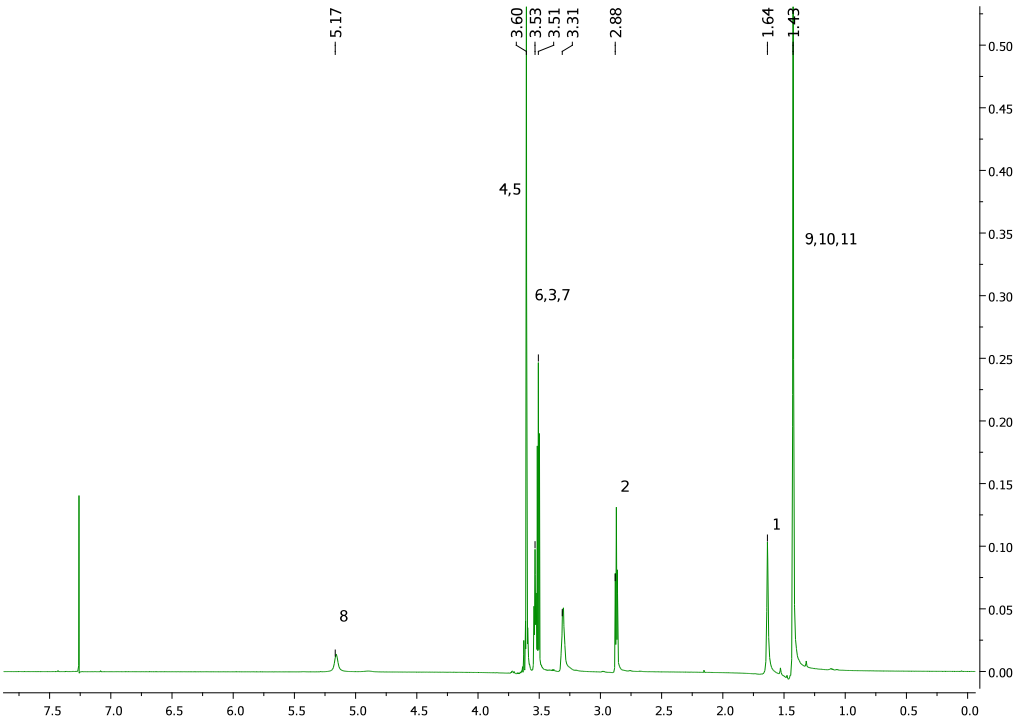

Figure S2. 1H-NMR spectrum of compound I

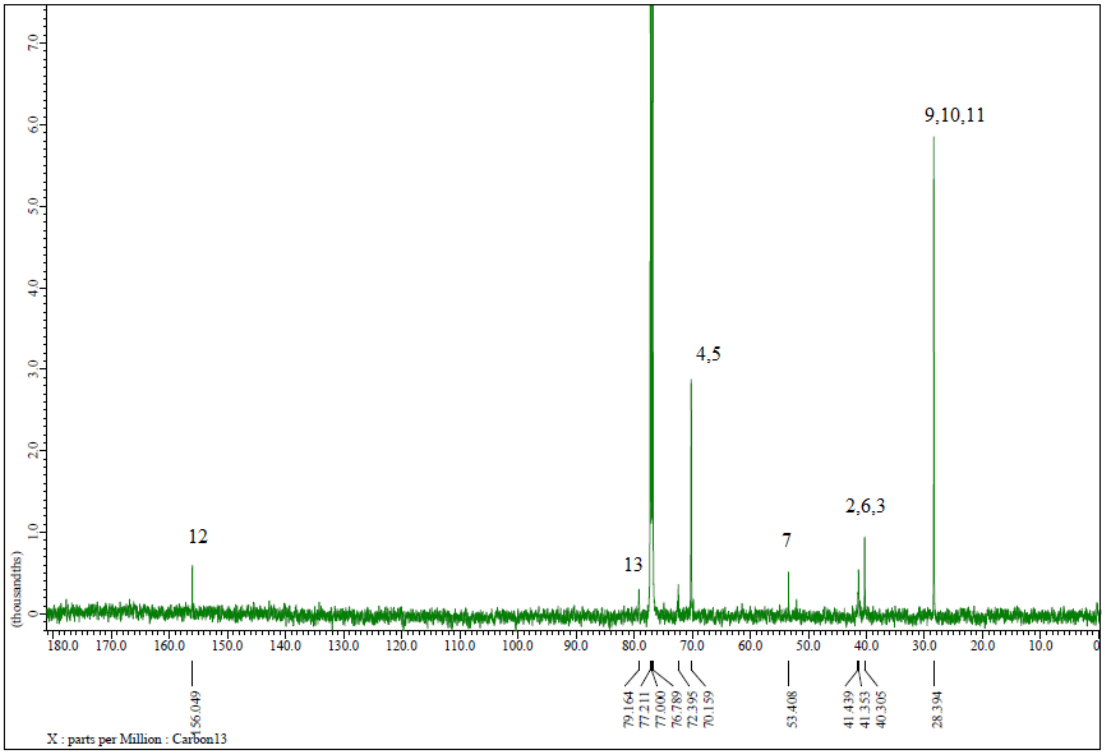

Figure S3. 13C-NMR spectrum of compound I

Characterization of tert-butyl-(2-(2-(2-((furan-2-yl-methyl)-amino)-ethoxy)-ethoxy)-ethyl)-carbamate (compound II):

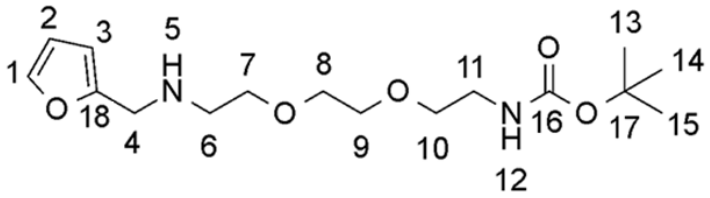

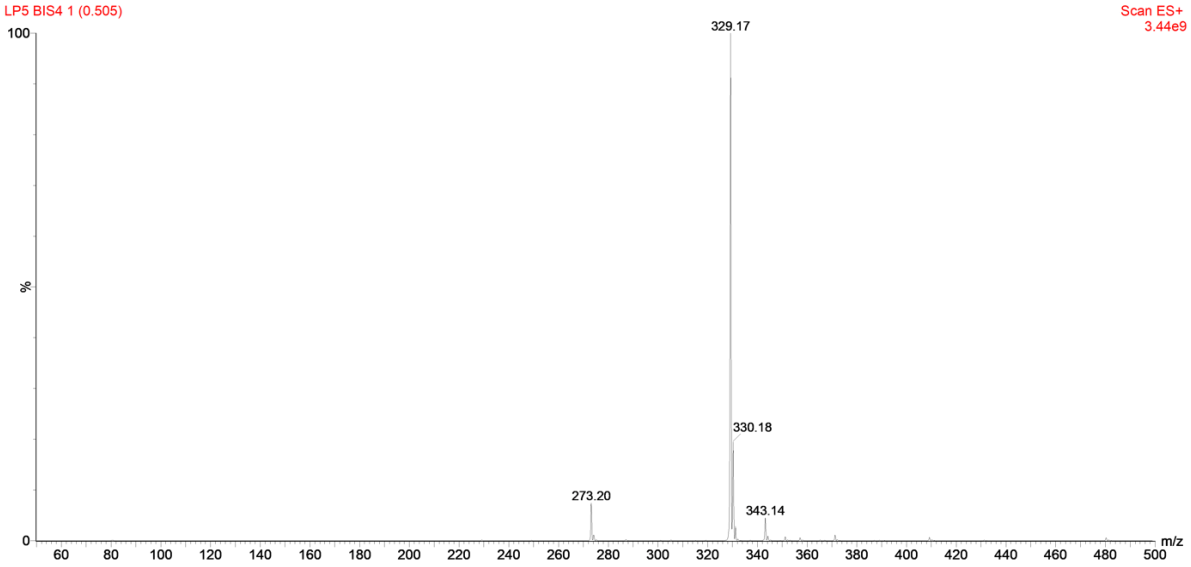

Figure S4. MS spectrum of compound II

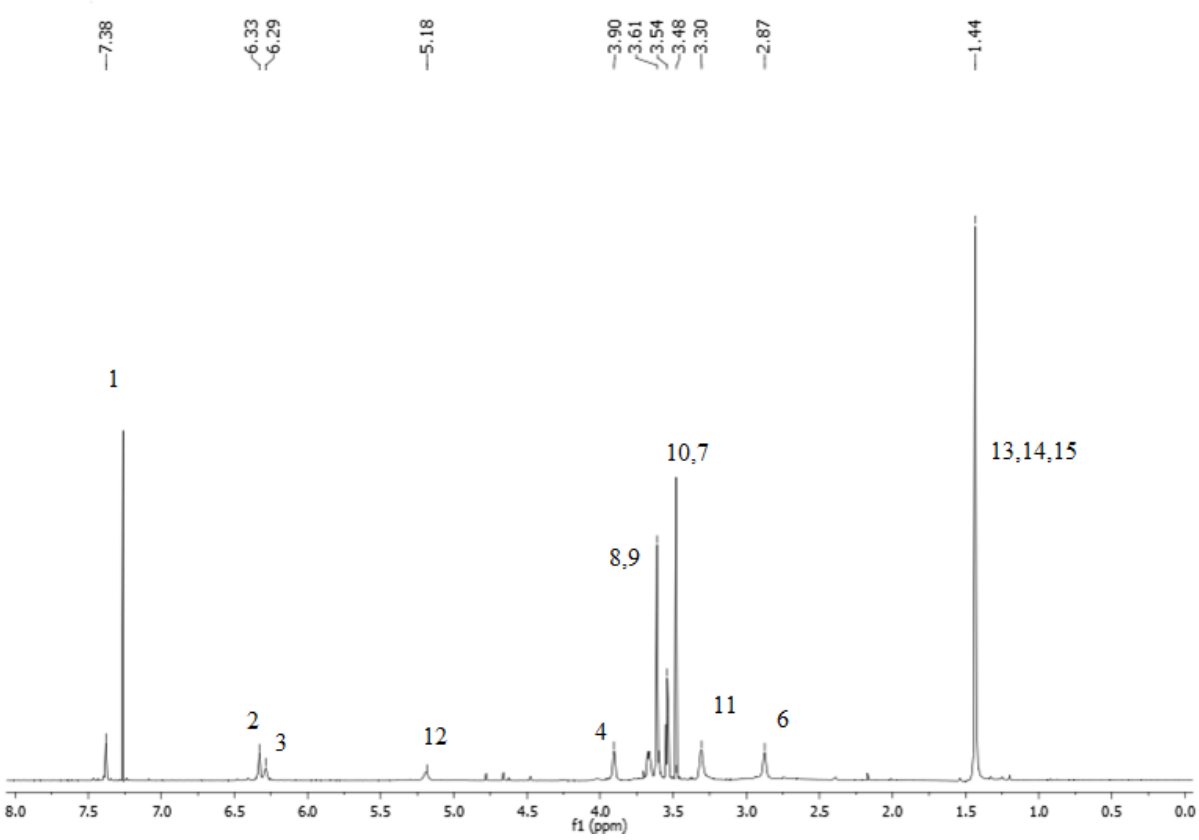

Figure S5. 1H-NMR spectrum of compound II

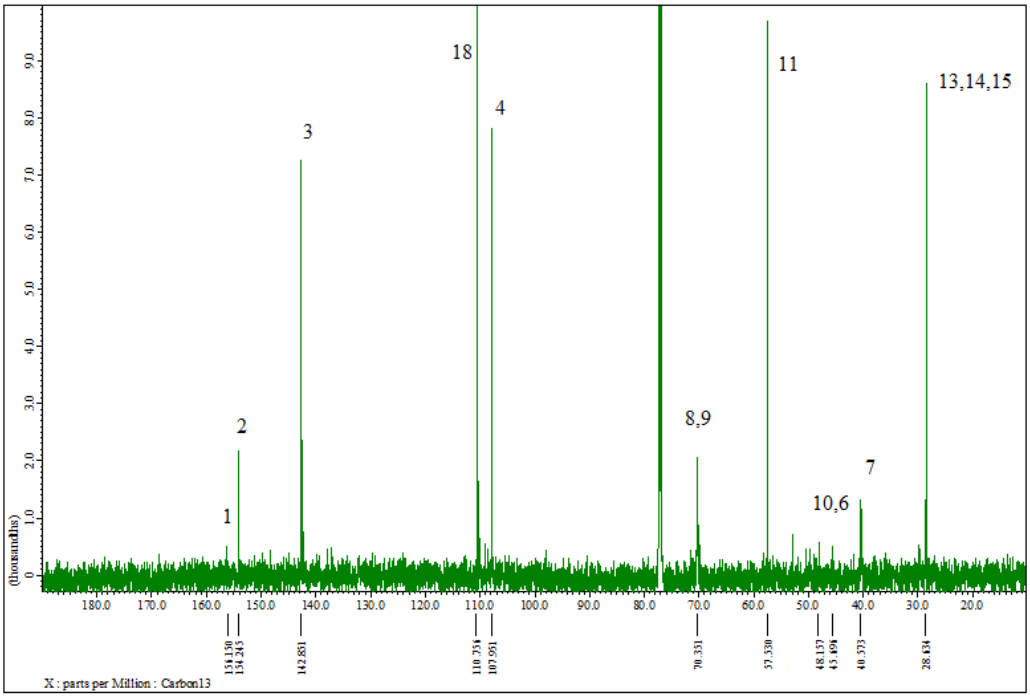

Figure S6. 13C-NMR spectrum of compound II

DRIFT characterization of nanodiamond

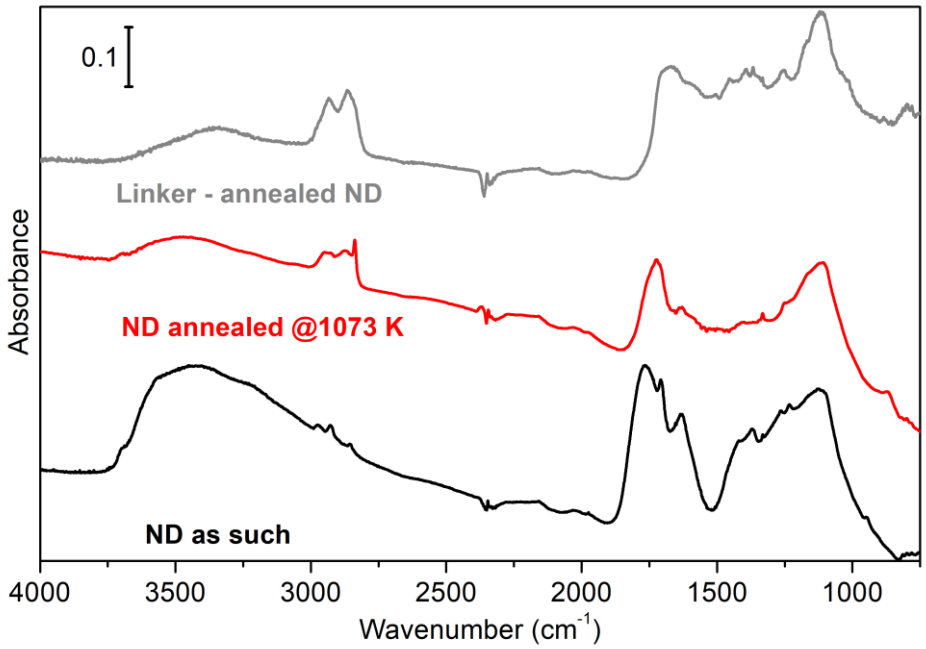

Figure S7. DRIFT spectra of untreated and annealed NDs

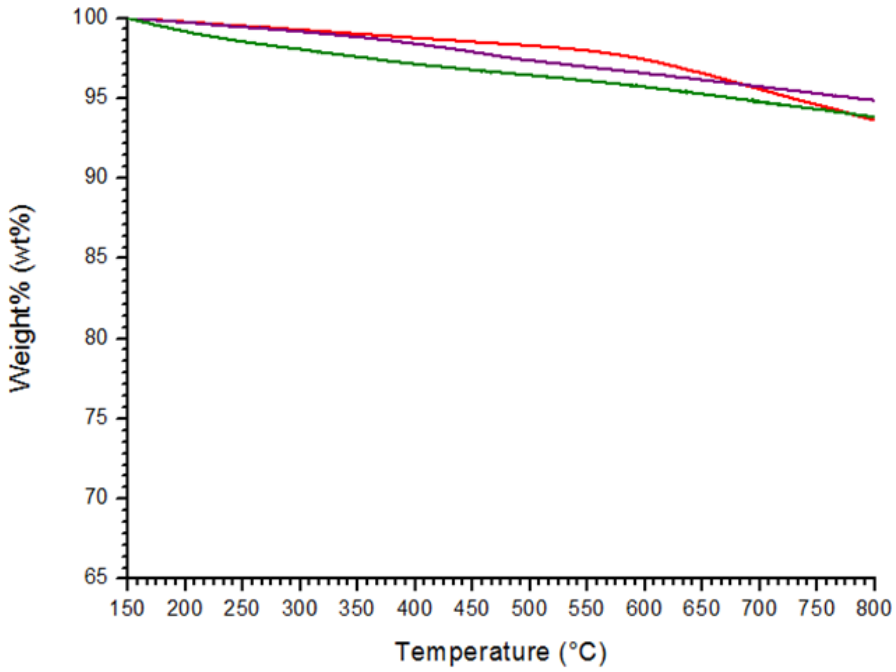

Figure S8 – Thermogravimetric analysis of annealed pristine ND (red);annealed NDs treated with porphyrin in the same conjugation reaction condition (purple); annealed NDs treated with porphyrin an EDC in the same conjugation reaction condition (green) NDs.